assuming no relativistic beaming. The timescale identified from the present observations is the time during which the dramatic 0.12 mag. variation occurred on 11 July 1987. The duration of this event is approximately 1.5 hours. If one uses the timescale of this event to define a 'characteristic timescale' and one assumes that the radiation is generated close to the black hole, for example $R = 3R_s$ where $R_s = 2GM/c^2$ is the Schwarzschild radius, then the mass of the supermassive black hole, M, is given by $M = c^3 t/6G = 1.42 \times 10^9\ M_\odot$. The Eddington luminosity for a black hole of mass M is given by[9] $L_E = 1.3 \times 10^{38}\ (M/M_\odot)$ erg s^{-1} which in this case yields $L_E = 1.85 \times 10^{47}$ erg s^{-1}. For a brightness of ~15.0 mag, the luminosity for BL Lac is of the order of $L_v \approx 10^{45}$ erg s^{-1}.

Thus we find that although microvariability is definitely present on very short timescales, which in turn suggests a very small source region, the luminosity of BL Lac is significantly less than the Eddington luminosity, and does not require relativistic beaming for its explanation.

We thank NOAO and Lowell Observatory for generous allocations of observing time. H.R.M. is grateful for support from the Research Grant Program at Georgia State University.

Received 19 September; accepted 20 December 1988.

1. Webb, J. R. *et al. Astr. J.* **95,** 374–397 (1988).
2. Racine, R. *Astrophys. J.* **159,** L99–103 (1970).
3. Kiplinger, A. L. *Astrophys. J.* **191,** L109–L110 (1974).
4. Miller, H. R. & McGimsey, B. Q. *Astrophys. J.* **220,** 19–24 (1978).
5. Moore, R. L. *et al. Astrophys. J.* **260,** 415–436 (1982).
6. Moore, R. L., Schmidt, G. D. & West, S. C. *Astrophys. J.* **314,** 176–186 (1987).
7. Howell, S. B. & Jacoby, G. J. *Publs astr. Soc. Pacif.* **98,** 802–808 (1986).
8. Carrasco, L., Dultzin-Hacyan, D. & Cruz-Gonzalz, I. *Nature* **314,** 146–148 (1985).
9. Wiita, P. J. *Phys. Rep.* **123,** 117–213 (1985).

A Solar System dust ring with the Earth as its shepherd

A. A. Jackson* & H. A. Zook†

* Lockheed Engineering and Science Corporation, C23, 2400 NASA Rd 1, Houston, Texas 77058-3711, USA
† SN3, NASA Johnson Space Center, Houston, Texas 77058, USA

Bodies orbiting in the gravitational fields of galactic, solar or planetary systems often suffer dissipative forces, including tidal interactions and drag resulting from motion through a gas or from collisions with dust grains. In the early solar nebula, gas drag induces resonance trapping, which may be of importance in the early accretional growth of planets[1–3]. By means of numerical integrations, we show here that small dust grains can be temporarily captured into exterior orbit–orbit resonances with the Earth, lasting from less than 10,000 years to more than 100,000 years. Grains with radii of 30–100 μm, orbiting in planes less than 10° from the plane of the Solar System and with orbital eccentricities of less than 0.3, are captured most easily. We argue that there should be an approximately toroidal cloud of particles, derived mostly from the asteroid belt, trapped into a variety of these exterior resonances. The cloud is mostly beyond the Earth's orbit, but includes it.

Three factors primarily motivated the present study. (1) The narrow bands observed along the ecliptic in the IRAS (Infrared Astronomical Satellite) data clearly seem to originate from dust particles in the main asteroid belt[4,5]; indeed, asteroid collisions may provide most of the dust grains that give rise to the entire broad band of observed zodiacal thermal emission[6]. (2) Grains smaller than ~100 μm in radius should successfully survive collisional destruction[7] to spiral in, under Poynting-Robertson[8] (P-R) and solar-wind drag, to well within the orbits of the Earth and Venus. (3) Venus and the Earth significantly perturb[9,10] the orbits (which are shrinking under P-R drag) of dust grains that pass these planets.

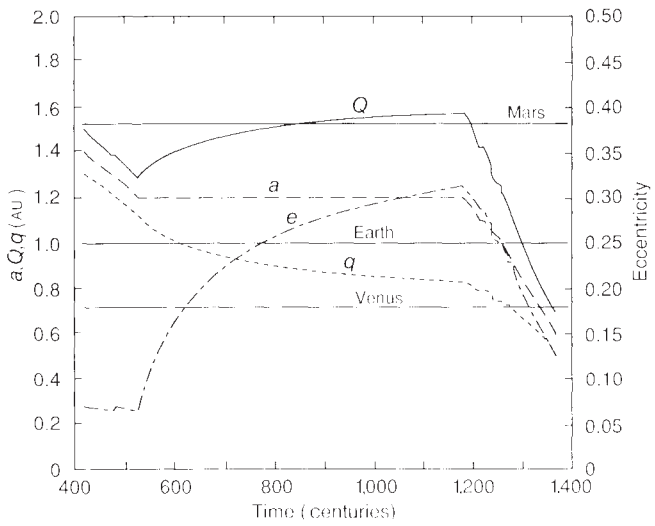

Fig. 1 Semi-major axis, a, aphelion distance, Q, perhelion distance, q, and eccentricity, e, as functions of time (in centuries) for a 30-μm radius particle started in an orbit with $a = 2.0$, $e = 0.1$ and an orbital inclination of 2.0°.

Some effects from dissipative forces in the Solar System have been noted. Gas drag, for example, can trap small bodies into $j:k$ orbital-period commensurabilities with a massive perturbing body (such as an accreting planet); here j and k are integers. Orbit-period commensurabilities of the type $j:j+1$ are often observed. Gonczi *et al.*[11] noted that, under P-R drag, small dust grains that were initiated in orbits at the interior 2:1 resonance with Jupiter could remain trapped there for some time; they did not, however, find any evidence for dust grains drifting, under P-R drag, into that resonance and becoming trapped.

Although our conclusions are consistent with those of Gonczi *et al.*, we also obtain new and different results (reported earlier in preliminary form[12]). These new results include long-term trapping (for more than 100,000 years) into resonances exterior to the Earth's orbit, short-term trapping (for typically less than 10,000 years) into resonances exterior to the orbits of Mars and Venus, and some limited trapping into interior resonances. For calculations we used Cowell integration in cartesian coordinates using the Everhart[13] implicit Runge-Kutta integrator with Gauss-Radau spacings. Radiation pressure is included and opposes the effect of solar gravity, with the assumption that particles behave as spherical black bodies of density 1 g cm^{-3}. The only other forces included are P-R drag and solar-wind drag, with the latter assumed to be 30% of the former. Solar-wind drag is included by multiplying by 1.3 the vector velocity term given by equation (5) in Burns *et al.*[14]. Many simulation runs incorporated the effect on the particles of the gravitational fields of the Sun, Venus, the Earth, Mars and Jupiter. To reduce computation, however, most runs included only the gravitational fields of the Sun, Venus and the Earth, and many were done with only those of the Sun and the Earth.

The trapping dynamics are best illustrated for the simplest case in which only the Sun, the Earth and a dust grain are involved. This case is shown in Fig. 1, where the orbital evolution of a particle of radius 30 μm is initiated with a semi-major axis, a, of 2.0 AU, an orbital eccentricity, e, of 0.1, and an orbital inclination of 2.0°. The plot starts at 40,000 years into the simulation. For the first 52,000 years, a decreases on average, under P-R and solar-wind drag, at a rate of 7.3 cm s^{-1}. The particle is then trapped into an external 3:4 resonance with the Earth at $a = 1.2037$ AU for the next 65,000 years; during this trapping period, a remains approximately constant, e increases, the perihelion distance, q, decreases to less than that of the

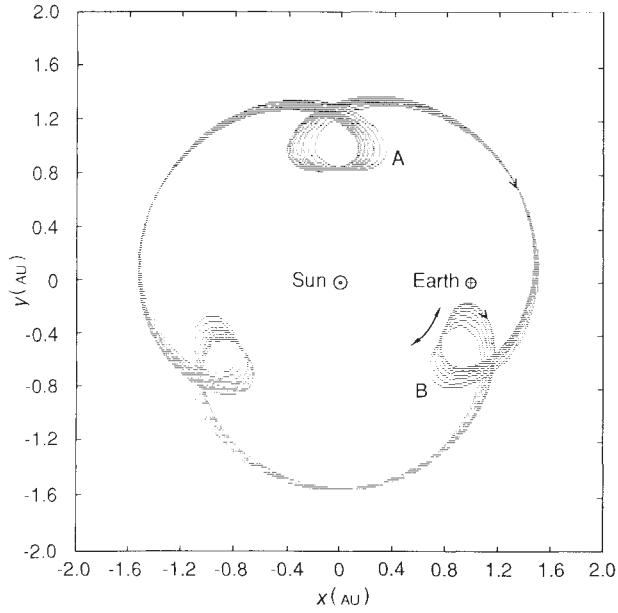

Fig. 2 The motion of the dust grain in Fig. 1, in a heliocentric coordinate frame rotating with the Earth. Shown here is the trajectory for 50 years of motion, projected onto the ecliptic, starting at 90,000 years into the simulation. The orbital motion tends to repeat itself in 220 years during quasi-stable trapping into the 3:4 external resonance with the Earth.

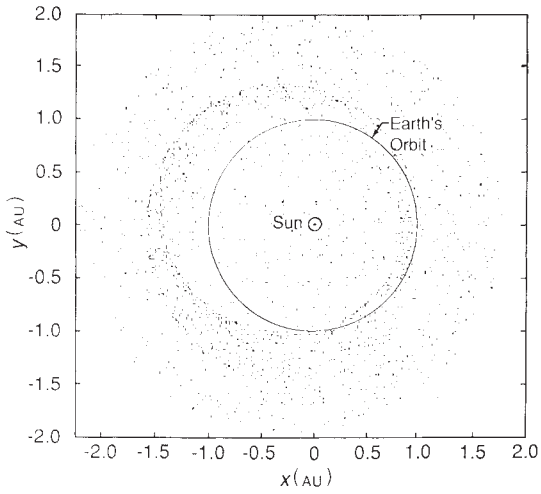

Fig. 3 The position of the particle for the orbit in Fig. 1, projected onto the ecliptic plane as a point approximately every 93 years as it evolves under gravitational and drag forces. The density enhancement arising from shepherding by the Earth is clearly evident.

Earth, and the aphelion distance, Q, increases. This trapping resonance is by no means unique: depending on the initial dust-grain orbital parameters, we have observed trapping in essentially all $j:j+1$ external resonances with the Earth from 2:3 to 13:14 (the latter for an initially circular orbit inclined at 10° to the ecliptic). We have also observed trapping into the 3:5 and 1:1 resonances. The 1:1 resonance resulted from the trapping of a 100-μm radius dust grain released from Comet Encke into a 'circulator' (rather than a horseshoe-shaped 'librator') resonance with the Earth.

Insight into the dynamics of the trapping can be obtained by transforming to a Sun-centred coordinate system rotating with the Earth's orbital motion. Figure 2 depicts particle motion, as viewed from ecliptic north, in such a coordinate system for 50 years, starting at 90,000 years into the same run as shown in Fig. 1. The Earth is shown to the right in this plot. At aphelion, the dust grain orbits more slowly around the Sun than does the Earth, and so moves in a clockwise fashion in this diagram. At perihelion, dust-grain orbital motion is faster than that of the Earth, and the grain moves in an anticlockwise direction. This pattern of motion gives rise to the three loops that are made during the four years that the particle takes to approximately retrace its path in this 3:4 resonance. The particle does not, however, exactly retrace its path on each orbit, because it is seldom precisely in the 3:4 resonance but only near it, in a quasi-stable trajectory, during the 65,000 years that it remains trapped. When the particle approaches relatively near, but trails orbitally behind, the Earth, just after particle perihelion passage, it receives a boost in orbital energy which increases its orbital semi-major axis a. If a becomes larger than the semi-major axis appropriate for the 3:4 resonance, then the dust grain has not quite completed three orbits by the time that the Earth has made four orbits. This causes the loops in the dust grain's orbit (Fig. 2) to drift in a clockwise direction. If this drift continues far enough, the gravitational downward 'kick' in the orbital energy of the dust grain can exceed the upward kick, because the dust grain now approaches closer to the Earth in loop A than in loop B. The orbital energy of the dust grain then decreases under both the Earth's gravitational force and the P-R and solar-wind drag forces until a becomes smaller than the resonance value. The loops then drift in an anticlockwise direction, and so on in a cyclic fashion. A high-resolution plot of semi-major axis against time clearly shows that a varies continuously throughout the trapping period to values both above and below the exact 3:4 resonance value of $a = 1.2037$.

In Fig. 3, we show the position of the particle projected as a point onto the ecliptic plane every 93.4377 years. It is clearly seen that the trapping phenomenon leads to an increased particle density near, but mostly outside of, a distance of 1 AU. The particle density is not uniform in heliocentric longitude because the line of apsides of the particle's orbit rotates by only ~180°, non-uniformly in time, during this particular trapping event. The orbital inclination of the particle in Figs 1, 2 and 3 remained near 2° throughout the trapping period, following which it varied rapidly to ~8°.

Large grains are trapped more easily into one of the external resonances than are small grains. Our numerical experiments have not generated a resonance with Mars for particle radii less than 60 μm. Large grains also tend to be trapped into resonances that have larger semi-major axes than those of small grains, and they stay trapped for longer periods of time. This can be explained by the relative rapidity with which small grains progress through a resonance trapping zone, a condition already noted for other types of trapping[15]. Grains with radii less than 10 μm are seldom trapped by the Earth or Venus and, when trapped, remain so only for very short periods. Grains of radius 30 μm are typically trapped exterior to the Earth for time spans of ~30,000 years, although they occasionally escape trapping altogether (even for orbits of low e and inclination). The overall physical process may be described as the 'shepherding' of dust grains into external orbit-orbit resonances by the combined perturbations of the Earth's gravity and P-R and solar-wind forces. Mars is a less effective trapper because of its small mass, and Venus loses trapping effectiveness primarily because of gravitational disturbances from the Earth.

The question now arises as to whether or not any observational evidence exists for the dust ring that we predict near the orbit of the Earth. There are two sets of observations that are consistent with, but not definitive proof of, a near-Earth dust ring. The first of these is the detection of micrometre- to sub-micrometre-sized meteoroids by the Pioneer 8 and 9 spacecraft. Zook[16] has suggested that these could be created by collisions in a

population of larger parent meteoroids whose spatial density increases with increasing heliocentric distance near 1 AU. McDonnell *et al.*[17], on the other hand, showed that the measurements could also be interpreted on the basis of a spatial density varying with heliocentric longitude. Which interpretation is correct should be resolved with the dust sensor on the Galileo spacecraft scheduled for launch in 1989.

The second set comprise zodiacal-light observations. In an examination of the zodiacal-light data gathered by the Helios spacecraft, Leinert *et al.*[18] failed to find the spatial-density increase suggested by Zook[16]. It is possible, however, that a low-intensity narrow ring near the Earth would not be easily detected by the photometers on Helios, because they did not make observations along the ecliptic plane. On the other hand, it may be significant that the spatial density of particles derived from zodiacal-light studies varies as $r^{-1.3}$ inside a radius of 1 AU (ref. 19) but as $r^{-1.5}$ or higher inverse powers[20,21] outside of this. Such a result could be caused by a dust ring near the Earth.

We thank Dr E. Everhart for sending us a copy of his numerical integration program and Dr Shin-Yi Su for independently programming and verifying the capture phenomena. We also greatly appreciate a review by Dr J. Burns.

Received 30 August; accepted 20 December 1988.

1. Greenberg, R. *Icarus* **33**, 62–73 (1978).
2. Weidenschilling, S. & Davis, D. *Icarus* **62**, 16–29 (1985).
3. Patterson, C. W. *Icarus* **70**, 319–333 (1987).
4. Low, F. J. *et al. Astrophys. J.* **278**, L19–L22 (1984).
5. Dermott, S. F., Nicholson, P. D., Burns, J. A., & Houck, J. R. *Nature* **312**, 505–509 (1984).
6. Sykes, M. V. & Greenberg, R. *Icarus* **65**, 51–69 (1986).
7. Grun, E. Zook, H. A., Fechtig, H. & Giese, R. H. *Icarus* **62**, 244–272 (1985).
8. Wyatt, S. P. & Whipple, F. L. *Astrophys. J.* **111**, 134–141 (1950).
9. Burkhardt, G. *Properties and Interactions of Interplanetary Dust* (eds Giese, R. H. & Lamy, P.) 389–393 (Reidel, Dordrecht, 1985).
10. Gustafson, B. A. S. & Misconi, N. Y. *Icarus* **66**, 280–287 (1986).
11. Gonczi, R., Froeschle, Ch. & Froeschle, Cl. *Icarus* **51**, 633–654 (1982).
12. Jackson, A. A. & Zook, H. A. *Lunar planet. Sci.* **XIX**, 539–540 (Lunar planet. Inst., Houston, 1988).
13. Everhart, E. *Dynamics of Comets: Their Origin and Evolution* (eds Carusi, A. & Valsecchi, G. B.), 185–202 (Reidel, Dordrecht, 1985).
14. Burns, J. A., Lamy, P. L. & Soter, S. *Icarus* **40**, 1–48 (1979).
15. Tittemore, W. C. & Wisdom, J. *Icarus* **74**, 172–230 (1988).
16. Zook, H. A. *Planet. Space Sci.* **23**, 1391–1397 (1975).
17. McDonnell, J. A. M., Berg, O. E. & Richardson, F. F. *Planet. Space Sci.* **23**, 205–214 (1975).
18. Leinert, C., Hanner, M. & Pitz, E. *Astr. Astrophys.* **63**, 183–187 (1978).
19. Leinert, C., Richter, I., Pitz, E. & Planck, B. *Astr. Astrophys.* **103**, 177–188 (1981).
20. Hanner, M. S., Sparrow, J. G., Weinberg, J. L. & Beeson, D. E. *Interplanetary Dust and Zodiacal Light* (eds Elsasser, H. & Fechtig, H.) 29–35 (Springer, Heidelberg, 1976).
21. Schuerman, D. W. *Solid Particles in the Solar System* (eds Halliday, I. & McIntosh, B. A.) 71–74 (Reidel, Dordrecht, 1980).

Detection of methyl, hydroxymethyl and hydroxyethyl hydroperoxides in air and precipitation

E. Hellpointner & S. Gäb

Gesellschaft für Strahlen- und Umweltforschung mbH München, Institut für Ökologische Chemie, D-8050 Freising-Attaching, FRG

It is well established that organic peroxides are formed by OH-radical-induced oxidation of hydrocarbons under atmospheric conditions[1]. Peroxyacyl nitrates have been known to be constituents of polluted air since the 1950s[2,3]. In a recent study we have shown that the gas-phase reaction of ozone with a variety of natural and anthropogenic alkenes can contribute to the formation of hydrophilic organic peroxides[4]. Indications that such peroxides are actually present in the environment have been obtained previously by measurements of the peroxide content of cloudwater and rain. In the absence of a specific analytical method the peroxide content after selective enzymatic destruction of the hydrogen peroxide was taken to be the organic peroxide fraction[5–7]. In this letter we report the determination by high-performance liquid chromatography of methyl (MHP; CH_3OOH), hydroxymethyl (HMP; $HOCH_2OOH$) and 1-hydroxyethyl (HEP; $CH_3CH(OH)OOH$) hydroperoxides, in addition to H_2O_2, and present some preliminary concentration ranges in air and precipitation. The existence of this class of atmospheric trace constituents raises questions about possible adverse biological effects.

Although reversed-phase high-performance liquid chromatography (HPLC) is one of the most important methods of separating polar compounds in aqueous solution, it has been little used in the search for products of tropospheric photooxidation. It is superior to gas chromatography in the detection of thermally unstable substances. The method described here (Fig. 1) exploits the stability of hydroxyalkyl hydroperoxides in cold acidic solution by using HPLC to separate them from H_2O_2, which is normally present in much higher concentrations. Directly after separation, both the temperature and the pH of the eluate are increased to convert the hydroxyalkyl hydroperoxides to H_2O_2 and the corresponding aldehydes. H_2O_2 is then detected by the highly specific and sensitive *p*-hydroxyphenyl ethanoic acid/peroxidase fluorescence reaction[8]. Any H_2O_2 initially present in the sample is eluted first from the HPLC column and is detected directly. MHP is also detected directly; it is stable to the higher temperature and pH, but reacts in the presence of horseradish peroxidase.

The peroxides were identified by comparison of their retention times with those of standards (Fig. 2 and Table 1) or by admixture of standards to the samples. The limit of detection is 0.07 μmol l^{-1}, corresponding to 1.4×10^{-6} μmol per 20 μl of

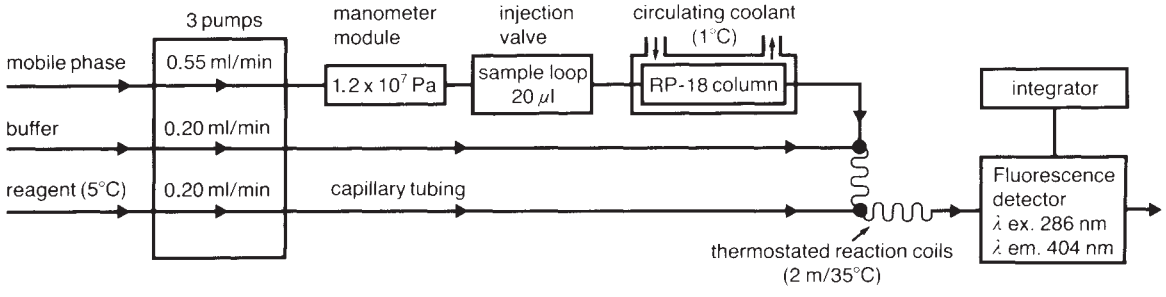

Fig. 1 Analytical system. HPLC: ABIMED, 3 Units Gilson model 302, 5 SC, Manometer module Gilson 802 C. Capillary tubing: o.d. 1/16", i.d. 0.12 mm. Injection valve: Rheodyne 7125. Cryostat: mgw Lauda K2R. Column: Bischoff Type NCi, 4×250 mm. Packing: 5-μm Shandon ODS Hypersil. Detector: Hewlett Packard HP 1046 A. Integrator: Hewlett Packard HP 3390. Water: deionized, distilled from $KMnO_4$, freed from traces of H_2O_2 with catalase, and redistilled. Mobile phase: diluted H_3PO_4, pH 3.5. Buffer: 0.01 M KH_2PO_4/NaOH, pH 9.4. Reagent: 0.5 mg *p*-hydroxyphenylethanoic acid (Merck) and 2 mg horseradish peroxidase (EC 1.11.1.7, ~170 U per mg, Merck) in 100 ml 0.01 M KH_2PO_4; 2 mg *p*-hydroxyphenylethanoic acid at peroxide concentrations > 10 μmol l^{-1}. At concentrations > 50 μmol l^{-1} the sample is diluted.